### Title
Fermi-surface evolution in Yb-substituted CeCoIn5




### Journal
Physical Review B, 85(24)

### ISSN
2469-9950



### Authors
Polyakov, A
Ignatchik, O
Bergk, B
et al.



### Publication Date
2012-06-15

### DOI
10.1103/physrevb.85.245119

# Fermi-surface evolution in Yb-substituted $CeCoIn_5$

A. Polyakov,[1] O. Ignatchik,[1] B. Bergk,[1] K. Götze,[1] A. D. Bianchi,[2] S. Blackburn,[2] B. Prévost,[2] G. Seyfarth,[2,3] M. Côté,[2] D. Hurt,[3] C. Capan,[3] Z. Fisk,[3] R. G. Goodrich,[4] I. Sheikin,[5] Manuel Richter,[6] and J. Wosnitza[1]

[1]*Hochfeld-Magnetlabor Dresden (HLD), Helmholtz-Zentrum Dresden-Rossendorf, D-01314 Dresden, Germany*

[2]*Départment de Physique and RQMP, Université de Montréal, Montréal, Canada H3C 3J7*

[3]*Department of Physics and Astronomy, University of California Irvine, Irvine, California 92697, USA*

[4]*Department of Physics, George Washington University, Washington, DC 20052, USA*

[5]*Laboratoire National des Champs Magnétiques Intenses, CNRS, UJF, F-38042 Grenoble, France*

[6]*Institut für Festkörper- und Werkstoffforschung (IFW) Dresden, PF 270116, D-01171 Dresden, Germany*

(Received 22 March 2012; published 19 June 2012)

We report results of systematic de Haas–van Alphen (dHvA) studies on $Ce_{1-x}Yb_xCoIn_5$ single crystals with varying Yb concentration. For $x = 0.1$, the well-known Fermi surfaces and the heavy effective masses of $CeCoIn_5$ ($x = 0$) have changed only slightly. We start to observe changes of the Fermi-surface topology at $x = 0.2$ leading to a drastic reconstruction above $x = 0.55$. At these concentrations, the effective masses are reduced considerably to values between 0.7 and 2.6 free electron masses. For both $YbCoIn_5$ and $CeCoIn_5$, the angular-resolved dHvA frequencies can be very well described by conventional density-functional theory calculations. Projection of the Bloch states onto atomic Yb-4$f$ orbitals yields a 4$f$ occupation of 13.7 electrons, in agreement with previous experimental results indicating an intermediate Yb valence of +2.3.

DOI: 10.1103/PhysRevB.85.245119 PACS number(s): 71.18.+y, 71.27.+a, 74.25.Jb

## I. INTRODUCTION

The interplay of partially filled 4$f$ or 5$f$ orbitals with conduction-band electrons is a key ingredient for the emergence of heavy-fermion behavior. The resulting Kondo resonances modify the electronic-excitation spectrum and the Fermi surface concomitant with heavy effective band-structure masses.[1] These correlated electrons may further lead to non-Fermi-liquid behavior and unconventional superconductivity often in conjunction with a quantum critical point (QCP), i.e., a zero-temperature phase transition tuned by some external control parameter such as pressure, magnetic field, or composition.[2] In this context, typical representatives are compounds containing the 4$f$ rare earths Ce and Yb.

One example is $CeCoIn_5$, an ambient-pressure superconductor with a record-high superconducting transition temperature for Ce-based compounds of $T_c = 2.3$ K.[3] A number of experimental facts point to an unconventional $d_{x^2-y^2}$ type of superconductivity (see Ref. 4 and references therein). There are indeed indications that $CeCoIn_5$ is close to an antiferromagnetic QCP, situated just on the low-pressure side, i.e., negative pressure would be needed to reach it.[5] As a unique feature, there exists a further magnetic-field-driven antiferromagnetic QCP near the upper critical field.[6–9] It has been speculated, that at an antiferromagnetic QCP the Fermi surface changes when the system crosses over from a normal antiferromagnetic metal to a strongly correlated Fermi liquid.[10] This makes our study of the influence of Yb doping on the Fermi surface in CeCoIn5 of particular interest.

At low temperatures with magnetic fields near $H_{c2}$, the phase transition from the normal to the superconducting state becomes first order[11] and a second superconducting phase appears at high magnetic fields and even lower temperatures.[12,13] This led to suggest that in $CeCoIn_5$ a Fulde-Ferrell-Larkin-Ovchinnikov (FFLO)[14,15] state is realized. Some recent neutron-diffraction results, however, show that in this phase antiferromagnetic order with a fixed magnetic wave vector appears,[16,17] which is in stark contrast to the expected ground state proposed by FF and LO.[18] This unusual but fascinating appearance of antiferromagnetism inside the superconducting phase is a challenge for our understanding and has led to considerable theoretical efforts.[19]

Besides pressure and magnetic field, substitutional changes on the different lattice sites in $CeCoIn_5$ have served as useful tuning parameters for the study of the quantum-critical behavior.[4,20–26] For example, an analysis of the entropy change between the normal and superconducting state combined with nuclear quadrupolar resonance seems to indicate that superconductivity is destroyed locally around the dopant center for substitutions on both the rare-earth as well as the indium site.[26] Moreover, the substitution on the rare-earth site has been found to influence the Kondo-lattice coherence and Cooper pairing in a rapid and uniform way.[20] Yb substitution, however, shows a different behavior[4,24,25] in that $T_c$ and the Kondo-coherence temperature do not scale, in contrast to other heavy-fermion compounds.[27] In its divalent state, Yb is expected to act as a nonmagnetic dilution destroying the Kondo coherence and superconductivity. Recent experiments, though, indicate[25] or have found evidence[24] for an intermediate valence of Yb in $Ce_{1-x}Yb_xCoIn_5$ that might explain the observed features.

In order to better understand the electronic properties of $Ce_{1-x}Yb_xCoIn_5$, we performed a detailed study of the Fermi surface and effective-mass evolution as a function of Yb concentration. High-quality single crystals with different Yb dilution were investigated by de Haas–van Alphen (dHvA) measurements. The experimentally observed Fermi-surface topology is in excellent agreement with the calculated band structure of $YbCoIn_5$. As evidenced by full-potential local-orbital (FPLO) calculations, the resulting valence of Yb is intermediate with +2.3. For small Yb concentration, $x = 0.1$, the effective masses remain strongly renormalized, whereas for $x \geqslant 0.2$ the masses are considerably reduced approaching the unrenormalized band-structure masses of $YbCoIn_5$.

 

## II. METHODS

The single crystals of $Ce_{1-x}Yb_xCoIn_5$ were grown from excess-In flux.[3] Details of their characterization can be found in Ref. 4. We have carefully measured the torque, $\vec{\tau} = \vec{M} \times \vec{B}$, caused by the anisotropic magnetization $M$ as a function of magnetic field $B$ for samples with nominal Yb concentrations of $x = 0$, 0.1, 0.2, 0.3, 0.5, 0.55, 0.85, 0.95, and 1. For these measurements, performed at the HLD in Dresden, we utilized capacitive cantilever torquemeters that could be rotated *in situ* around one axis. The cantilevers were mounted either inside a $^3$He cryostat equipped with a 15-T superconducting magnet or in the $^3$He/$^4$He mixture of a toploading dilution refrigerator inside a 20-T superconducting magnet. We could resolve dHvA oscillations for the samples with $x = 0$, 0.1, 0.55, 0.85, 0.95, and 1.

In extension of this study, we performed further high-field torque measurements at the Grenoble branch of the Laboratoire National des Champs Magnétiques Intenses. The samples with $x = 0.1$ and 0.2 were measured up to 35 T in a toploading dilution refrigerator equipped as well with a rotatable capacitive cantilever. This extended field range allowed us to resolve magnetic quantum oscillations for $x = 0.2$ as well as additional dHvA frequencies for $x = 0.1$.

Band-structure calculations were done in the framework of density-functional theory (DFT) with a generalized gradient approximation for the exchange-correlation energy functional[28] using the ABINIT code in the projector augmented wave formalism.[29] The wave functions were expressed with a plane-wave basis up to an energy cutoff of 40 Ha (1088 eV). The Brillouin zone was sampled with a $16 \times 16 \times 16$ $k$-points grid. The crystal structures were fully relaxed. The calculated unit-cell parameters are found to be 1.1% smaller than experimental data in $YbCoIn_5$ and 1.5% in $CeCoIn_5$.[30]

To obtain a more detailed description of the electronic structure in the Brillouin zone, maximally localized Wannier functions[31] were constructed which allowed to interpolate the Fermi surface on a very fine $k$-points grid and, hence, calculate the area of cross sections of the Fermi surface efficiently and precisely. Typically, a grid of $800 \times 800$ was used to determine the area of a Fermi surface. The interpolated $k$ grid for the calculation of the cross-section area of the Fermi surface is refined up to an accuracy of $10^{-4}$ Å$^{-2}$ which corresponds to 10 T on the dHvA frequency.

The occupation of the Yb-4$f$ states was evaluated with the full-potential local-orbital (FPLO) code,[32,33] version 9.01, using the same parametrization of the exchange-correlation functional as in the ABINIT calculations and experimental structure parameters.[30] The FPLO valence basis set comprised the following states: Yb-4$f$, 5$s$, 5$p$, 5$d$, 5$f$, 6$s$, 6$p$, 6$d$, 7$s$; Co-3$s$, 3$p$, 3$d$, 4$s$, 4$p$, 4$d$, 5$s$; In-4$s$, 4$p$, 4$d$, 5$s$, 5$p$, 5$d$, 6$s$, 6$p$. A linear tetrahedron method with Blöchl corrections with a **k** mesh of $33 \times 33 \times 20$ points in the full Brillouin zone was used for the **k**-space integrations. Spin-orbit coupling was included by employing a full relativistic four-component mode.

## III. RESULTS AND DISCUSSION

We measured the field-dependent magnetic torque for nine different Yb concentrations and could observe magnetic quantum oscillations in seven of them. The as-measured torque signals for eight $Ce_{1-x}Yb_xCoIn_5$ samples up to 18 T are shown in Fig. 1. The magnetic field was aligned along (or slightly off) the $c$ axis. For the samples with Yb concentrations up to $x = 0.55$, clear anomalies appear in the torque at the upper critical fields. As was found already earlier,[4,25] the superconducting transition temperature and the upper critical field are only weakly suppressed with $x$. This contrasts other rare-earth substitutions of Ce in $CeCoIn_5$.[20] For $x = 0.85$ and above, no signs of superconductivity are visible any more.[4]

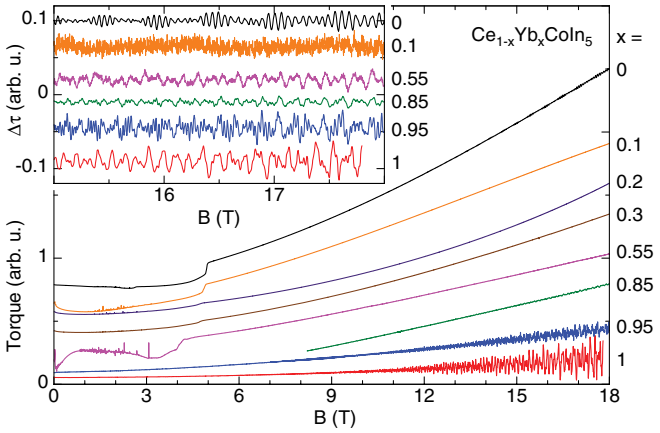


FIG. 1. (Color online) Magnetic-field dependence of the torque signals for $Ce_{1-x}Yb_xCoIn_5$ samples with different $x$. For Yb concentrations up to $x = 0.55$ the upper critical fields are visible as steplike features. The field was aligned along the $c$ axes, except for the sample with $x = 0.55$ where the field was tilted by $\Theta_{010} = 2^\circ$. The inset shows the oscillating dHvA signals after subtracting smooth backgrounds from the torque data. For $x = 0.55$, data for $\Theta_{010} = 7^\circ$ are shown. The data were measured at different temperatures between 25 and 75 mK.

In the normal state, the torque signals show approximately a $B^2$ dependence, that is expected for paramagnetic materials where $M \propto B$. On top of this background signal, oscillating dHvA signals can be resolved for the pure samples as well as for the samples with Yb concentrations of $x = 0.1$, 0.55, 0.85, and 0.95. This becomes clearer after background subtraction (using fourth-order polynomials) in the inset of Fig. 1. The observation of dHvA signals proves the high quality of the samples.

The spectral richness of the oscillating signals can be realized in the Fourier spectra shown in Fig. 2. For the Fourier transformations over the high-field range between 15 and 18 T [Fig. 2(a)], dHvA frequencies can be resolved for all six concentrations. The compounds with Yb concentrations between 1 and 0.55 show a very similar spectral composition of their dHvA oscillations. Then again, for the materials with $x = 0.1$ and pure $CeCoIn_5$, the spectrum has changed clearly. This proves distinctly different Fermi surfaces for these two Yb concentration ranges.

When extending the field range for the Fourier transformations down to 8.5 T [Fig. 2(b)], the increased spectral resolution allows to disentangle about 13 fundamental dHvA frequencies for the Yb-rich concentrations (labeled $F_1$ to $F_{13}$) and about

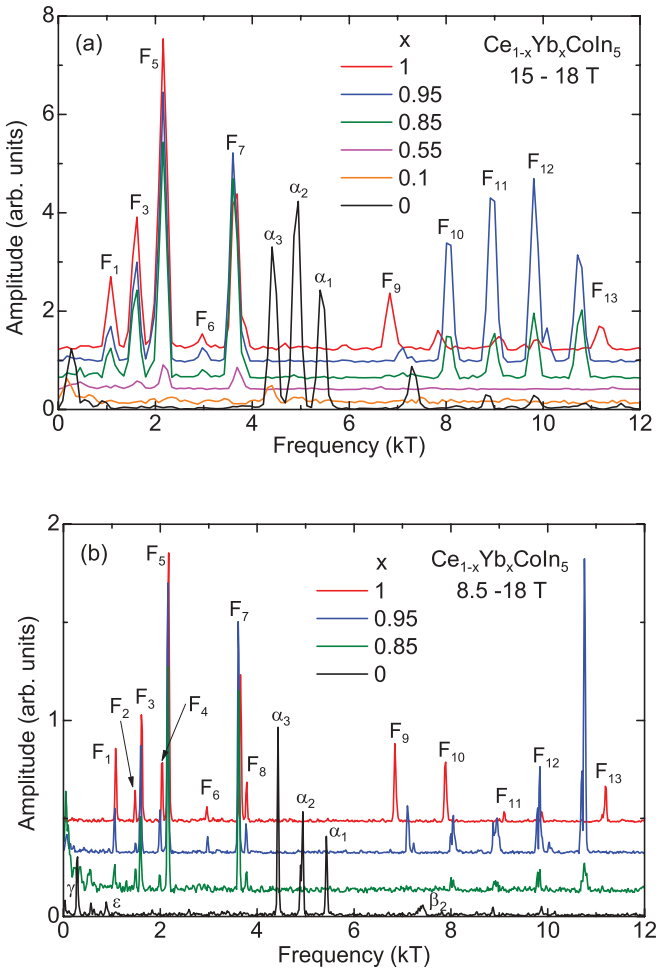


FIG. 2. (Color online) Fourier spectra of the background-subtracted torque signals shown in the inset of Fig. 1 taken between (a) 15 and 18 T and (b) 8.5 and 18 T.

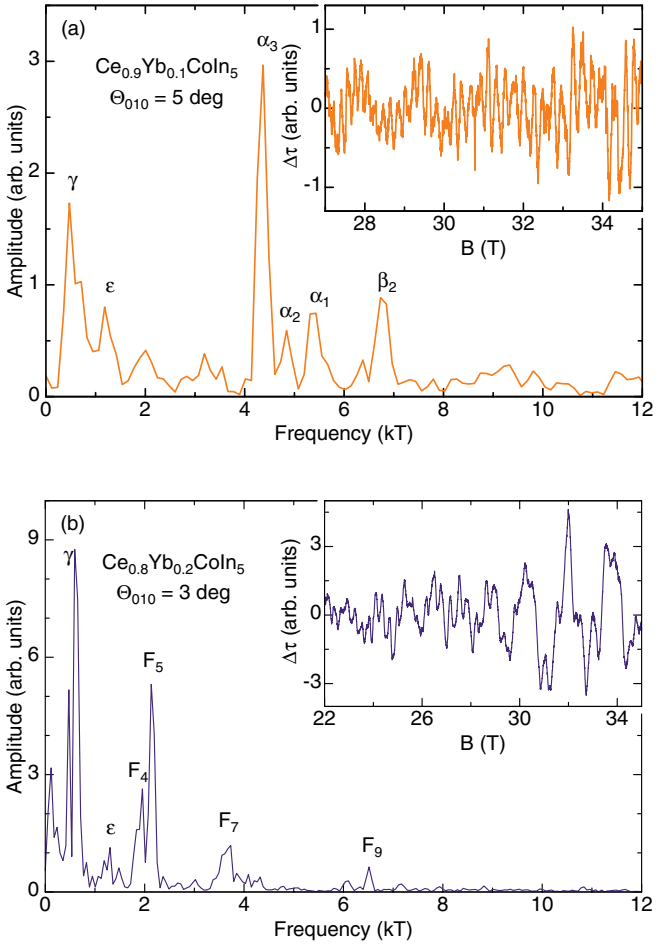


FIG. 3. (Color online) Fourier spectra of the background-subtracted torque signals shown in the insets for (a) $Ce_{0.9}Yb_{0.1}CoIn_5$ and (b) $Ce_{0.8}Yb_{0.2}CoIn_5$. The data were collected at 30 mK.

seven fundamental frequencies for $CeCoIn_5$. For the latter, the strongest spectral peaks are labeled $\alpha_1$ to $\alpha_3$ according to the assignment of earlier studies to which we find very good agreement both in the dHvA frequencies as well as in the effective masses (discussed below).[34,35]

In our measurements up to 20 T, we could just barely resolve dHvA signals for $Ce_{0.9}Yb_{0.1}CoIn_5$ [inset of Figs. 1 and 2(a)] and no oscillations for the samples with Yb concentrations of $x = 0.2$, 0.3, and 0.5. For that reason, we extended the magnetic-field range up to 35 T in a 1-week experiment at the Grenoble High Magnetic Field Laboratory. By that, we were able to detect dHvA oscillations for the sample with $x = 0.2$ and a number of additional dHvA frequencies for $x = 0.1$.

The oscillating torque signals for these two samples for magnetic fields applied 5° or 3° off the $c$ direction are shown in the insets of Fig. 3. The Fourier transformations (main panels of Fig. 3) allow to disentangle at least six dHvA frequencies for each compound. The spectral distribution of these frequencies is, however, clearly different for the two concentrations. Whereas for $x = 0.1$ the spectrum is almost identical to that of the pure $CeCoIn_5$ sample, the dHvA spectrum for $x = 0.2$ has obviously changed. For the latter, the $\alpha$ orbits between 4 and 6 kT are absent and new orbits at 2 kT appear [labeled $F_4$ and $F_5$ in Fig. 3(b)]. On the other side, the dHvA frequencies below 1000 T are only seen for Ce-rich samples. Consequently, for $x = 0.2$ the dHvA frequency spectrum reflects a mixture of $CeCoIn_5$ and $YbCoIn_5$ band structures.

Upon rotating the samples, we carefully measured the angular dependences of the dHvA frequencies (Fig. 4). From that, some principal features of the Fermi-surface topologies can be extracted. We may categorize the observed angular changes as follows. The low-frequency dHvA signals $F_1$ and $F_2$ in the Yb-rich samples are observable for almost all field orientations with nearly constant frequencies, i.e., for rotations around the [010] direction, $\Theta_{010}$, as well as around the $c$ axis, $\Theta_{001}$.[36] The same statement can be made for the $\epsilon$ and $\gamma$ orbits in $CeCoIn_5$ and in the samples with $x = 0.1$ and 0.2. This correlates with one strongly corrugated or two small closed three-dimensional Fermi surfaces. Other dHvA frequencies ($F_3$ to $F_9$) can be traced over an extended angular range and follow roughly a $1/\cos(\Theta)$ dependence, where $\Theta$ here is the angle with respect to the $c$ axis. The dashed line in Fig. 4(f) visualizes this dependence. Such kind of behavior (similar for $\alpha_1$ to $\alpha_3$ in $CeCoIn_5$ and $Ce_{0.9}Yb_{0.1}CoIn_5$) is evidence for quasi-two-dimensional Fermi-surface sheets. The other dHvA frequencies disappear quickly when rotating away from the

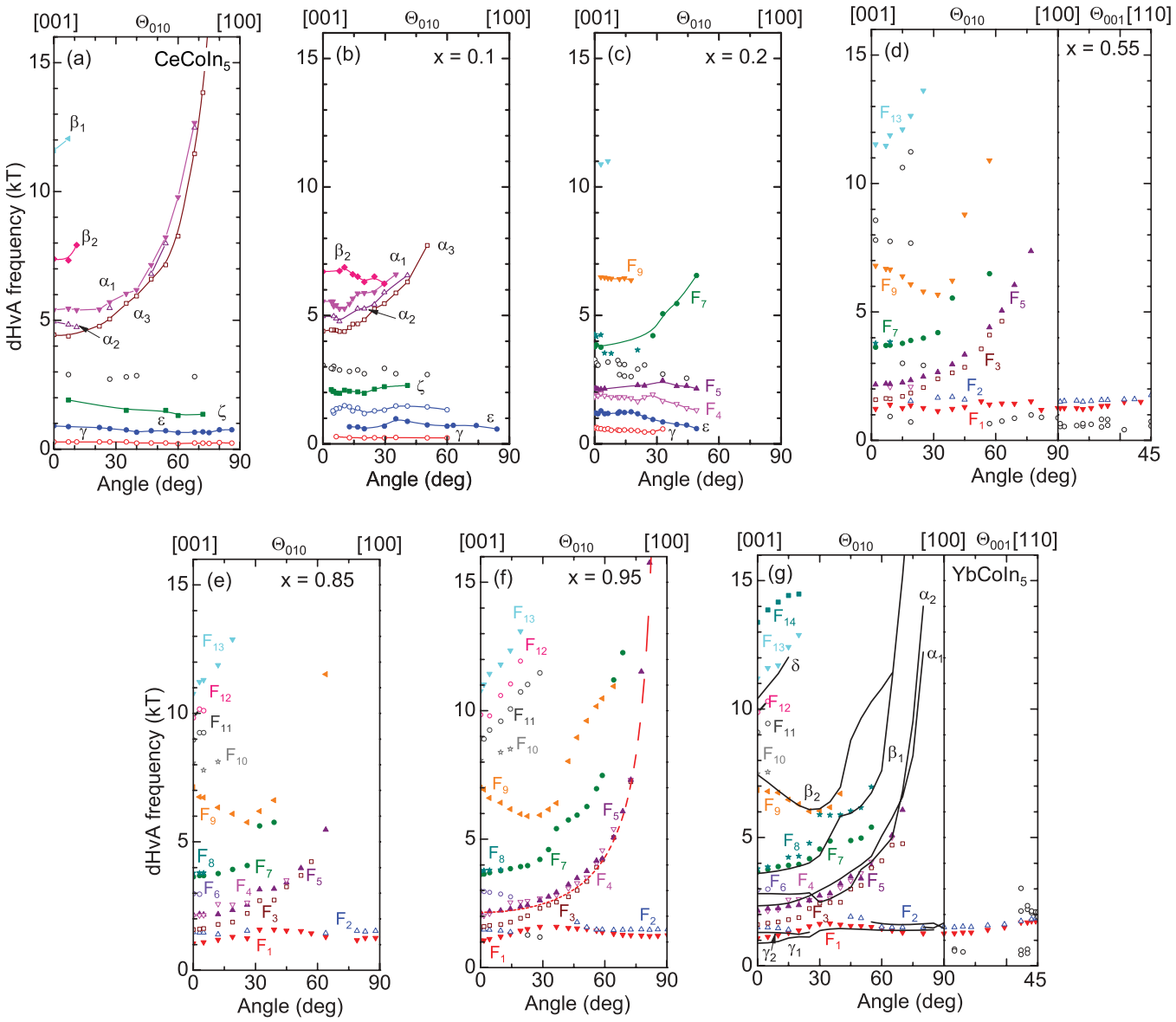


FIG. 4. (Color online) Angular dependences of the observed dHvA frequencies for (a) $CeCoIn_5$, (g) $YbCoIn_5$, as well as for different Yb concentrations (b)–(f). The solid lines in (g) correspond to the extremal orbits shown in the calculated Fermi surface of $YbCoIn_5$ depicted in Fig. 5. The dashed line in (f) shows a $1/\cos(\Theta)$ dependence.

*c* axis. Since the amplitudes of the dHvA signals are quite large, this indicates complicated, probably multiconnected Fermi-surface sheets.

The Fermi surfaces shown in Fig. 5 with some highlighted extremal orbits from *ab initio* DFT calculations account for the measured dHvA signals in $YbCoIn_5$. The found topologies are very similar to calculated Fermi surfaces of other 115 compounds without $4f$ contributions to the band structure.[37] The calculated angular dependences of the corresponding dHvA frequencies are shown as the solid lines in Fig. 4(g). Obviously, the frequencies $F_1$ and $F_2$ originate from the orbits $\gamma_1$ and $\gamma_2$ of the closed, highly deformed Fermi-surface sheet centered around Γ. A corrugated cylindrical Fermi surface at the corner of the Brillouin zone gives rise to the frequencies $F_3$ to $F_6$. Two of the extremal orbits are sketched as $\alpha_1$ and $\alpha_2$ in Fig. 5. Another highly corrugated Fermi surface surrounding the former warped cylinder explains with the orbits $\beta_1$ and $\beta_2$ the frequencies $F_7$ [and probably as well the satellite $F_8$—see Fig. 2(b)] and $F_9$. The final calculated multiconnected Fermi surface accounts with the shown $\delta$ orbit for the dHvA frequency $F_{13}$. It may be responsible as well for some other experimentally observed dHvA frequencies. The complicated topology of this Fermi surface, however, leaves a definite assignment ambiguous.

With decreasing Yb concentration, we observe only small changes of the dHvA frequencies, i.e., of the Fermi surfaces of $x = 0.95$, 0.85, and 0.55 [Figs. 4(f)–4(d)]. The low-frequency dHvA spectra (Fig. 2) remain almost unchanged, whereas the higher frequencies belonging to the $\beta$ and multiconnected Fermi-surface sheets move slightly (Fig. 2). The clear observation of these changes, especially of the different shifts of the low- and high-frequency dHvA spectra, reflects the true

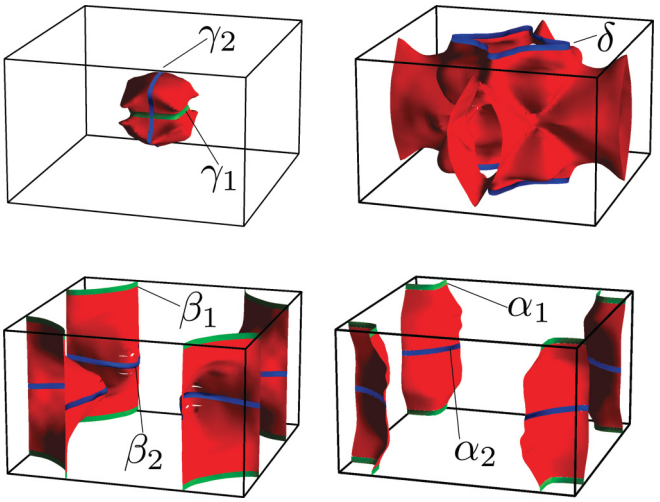


FIG. 5. (Color online) Fermi surface for $YbCoIn_5$ from DFT calculations. The blue and green lines are orbits of extremal area. Corresponding de Haas–van Alphen frequencies are reported in Fig. 4(g).

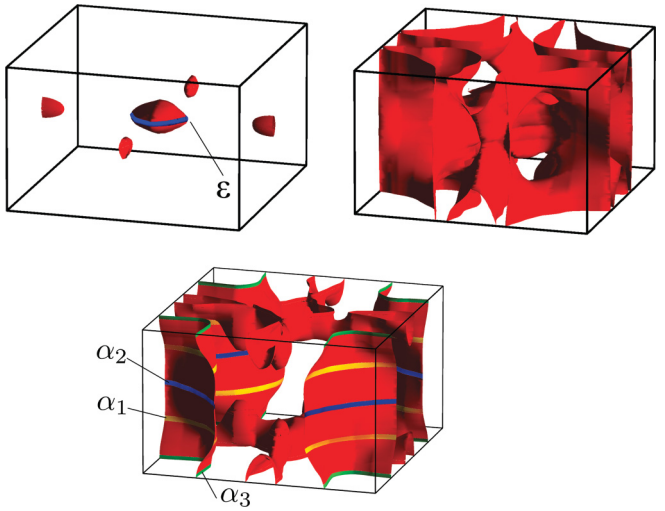


FIG. 6. (Color online) Fermi surface for $CeCoIn_5$ from DFT calculations. The lines depict orbits of extremal area. Corresponding experimental data are shown in Fig. 4(a).

substitution of Yb by Ce and renders a phase separation in the samples unlikely.

Recent x-ray absorption spectroscopy experiments provided evidence for an intermediate-valence state of $Yb^{2.3}$ in $YbCoIn_5$.[24] As a reminder, $Yb^2$ corresponds to a closed $4f$ shell, whereas $Yb^3$ corresponds to a $4f^{13}$ configuration. In order to check the compatibility of this finding with the present data and calculations, we evaluated the Yb-$4f$ occupation, $n_{4f}$, using the FPLO code and found $n_{4f} = 13.7$. Thus, the occupation number found in the present ordinary density-functional calculations using the generalized gradient correction is in accordance with the previously measured intermediate valence state.

Clearly different Fermi surfaces are apparent for the Ce-rich samples with $x = 0$ and 0.1 [Figs. 4(a) and 4(b)]. There are two low-frequency dHvA signals, $\gamma$ and $\epsilon$, that probably arise from two small ellipsoidal Fermi surfaces around the $\Gamma$ and $X$ points (Fig. 6 and Ref. 34). The $\alpha$ orbits showing a quasi-two-dimensional angular dependence can be explained by a corrugated cylindrical Fermi surface that has approximately twice the area compared to the $\alpha$ sheet in $YbCoIn_5$. The $\beta_1$ and $\beta_2$ frequencies can be assigned to orbits of a complicated multiconnected Fermi surface with strongly renormalized heavy masses.[34] As mentioned, the sample with $x = 0.2$ reveals dHvA frequencies composed of both kinds of Fermi-surface topologies.

From the temperature dependences of the dHvA oscillation amplitudes the effective cyclotron masses $m^*$ have been determined for selected angles. Some typical data for the $\alpha$ and $F_7$ orbits are shown in Fig. 7 (see also Table I), along with their fits and corresponding effective masses, according to the Lifshitz-Kosevich theory.[38,39] It is immediately evident that the dHvA signals for the Ce-rich samples diminish very quickly with temperature corresponding to large effective masses of roughly ten times the free-electron mass $m_e$.[40] This reflects the strong renormalization of the masses due to many-body interactions. It should be mentioned that, in line with our findings, a considerable field, spin, and angular dependence of the effective masses in $CeCoIn_5$ was found.[34,35] This reflects that Kondo physics is relevant and that possibly quantum critical fluctuations also play a role.

As opposed to low Yb concentrations, the effective masses of samples with concentrations of $x = 0.55$ and above are considerably smaller, i.e., only about $1.4m_e$, allowing to observe the dHvA signals up to much higher temperatures. Indeed, the effective masses for all observed bands in materials of this Yb concentration range are small and lie between $0.7m_e$ and $2.6m_e$ which clearly shows that heavy-fermion physics is not an issue here.[41] For the sample with $x = 0.2$, we as well find only relatively light effective masses in the range of $2m_e$–$5m_e$ for the observed orbits at 32 T.[42]

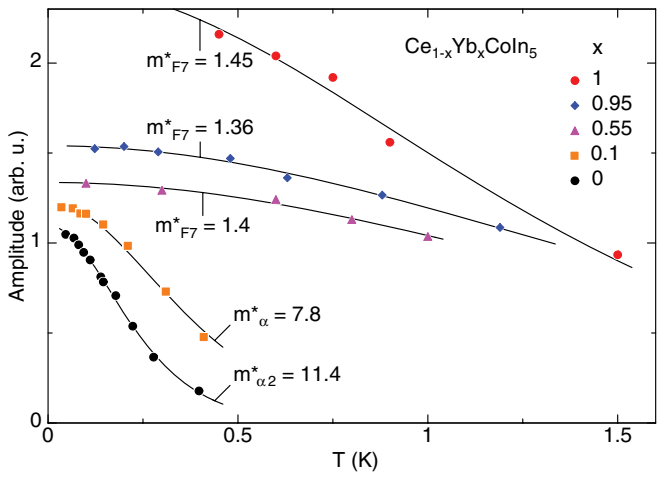


FIG. 7. (Color online) Temperature dependence of the dHvA amplitudes for selected orbits and Yb concentrations. The solid lines are fits using the Lifshitz-Kosevich formula yielding the noted effective masses in units of the free-electron mass. The data were obtained at the following angles, $\Theta_{010}$, and average magnetic fields: At 0° and 11.9 T for $x = 1$; 0° and 15.8 T ($x = 0.95$); 15° and 16.4 T ($x = 0.55$); 14° and 19 T ($x = 0.1$); 7° and 17 T ($x = 0$).

TABLE I. dHvA frequencies and effective masses for various extremal orbits in $YbCoIn_5$ and $CeCoIn_5$ for a magnetic field in the [001] direction from experiment and calculations.

| | | $F$ (kT) | | $\lvert m^*\rvert$ ($m_e$) | |
|---|---|---|---|---|---|
| Sample | Orbit | Expt. | Calc. | Expt. | Calc. |
| $YbCoIn_5$ | $\gamma_1$ | 1.08 | 0.9 | 0.96 | 0.5 |
| | $\gamma_2$ | 1.5 | 1.3 | [a] | 0.8 |
| | $\alpha_1$ | 2.04 | 2.3 | 0.7 | 0.5 |
| | $\alpha_2$ | 2.96 | 2.8 | [b] | 0.8 |
| | $\beta_1$ | 3.66 | 3.6 | 1.5 | 1.0 |
| | $\beta_2$ | 6.84 | 7.4 | 1.2 | 1.0 |
| | $\delta$ | 11.2 | 10.4 | 1.3 | 1.1 |
| $CeCoIn_5$ | $\alpha_1$ | 5.46 | 5.6 | 14.5 | 1.5 |
| | $\alpha_2$ | 4.87 | 4.7 | 11.4 | 1.2 |
| | $\alpha_3$ | 4.37 | 3.9 | 9.3 | 1.3 |

[a]The nearby frequency $F_3$ (Fig. 2) did not allow to determine the effective mass of the $\gamma_2$ ($F_2$) orbit experimentally.
[b]The weak dHvA amplitude prevented a reliable effective-mass determination ($F_6$ in Fig. 2).

From the DFT calculations, we find effective masses for a magnetic field along the $c$ direction to be near 1 $m_e$ as reported in Table I. These are calculated using

$$m^* = \frac{\hbar^2}{2\pi}\left(\frac{\partial A}{\partial \epsilon_F}\right), \tag{1}$$

where $A$ is the area of the Fermi surface cross section. For $YbCoIn_5$, the experimental values are only slightly larger, most probably due to many-body interactions.

The band structure depicted in Fig. 8(a) shows that the Yb-$f$ density of states peaks 0.5 eV below the Fermi energy. It is almost zero at the Fermi level where the most significant contribution is from Co-$d$ orbitals. We find that including spin-orbit coupling does not change the band structure near the Fermi level despite the proximity of the $f$ electrons.

In $CeCoIn_5$, the calculated frequencies are 5.6, 4.7, and 3.9 kT for the $\alpha_1$, $\alpha_2$, and $\alpha_3$ orbits, respectively, for fields along the $c$ direction. These values are in good agreement with the experimental data. Similar to $YbCoIn_5$, we find that spin-orbit coupling does not affect much the Fermi surface. The associated effective masses are much lower than the experimental data (Table I). The partially filled Ce-$f$ orbitals [Fig. 8(b)] are expected to be strongly correlated, therefore not correctly described by our calculations. This explains why we find the correct Fermi surface but lower effective masses. Adding a Hubbard term on localized orbitals such as it is done in DFT + $U$, is known to improve the agreement between theory and experimental data for compounds with $f$ electrons.[43] More sophisticated approaches, such as DFT + DMFT (dynamical mean field theory), could also improve our results.[44] It remains to be seen if such methods could improve the agreement of the effective masses for $CeCoIn_5$, but this falls outside of the scope of the present study.

The Yb-concentration dependence of the measured effective masses contradicts the specific-heat results reported in Refs. 4 and 25 where up to $x = 0.55$ almost no change of the Sommerfeld coefficient and for higher concentrations up to $x = 0.8$ only a moderate reduction of the electronic

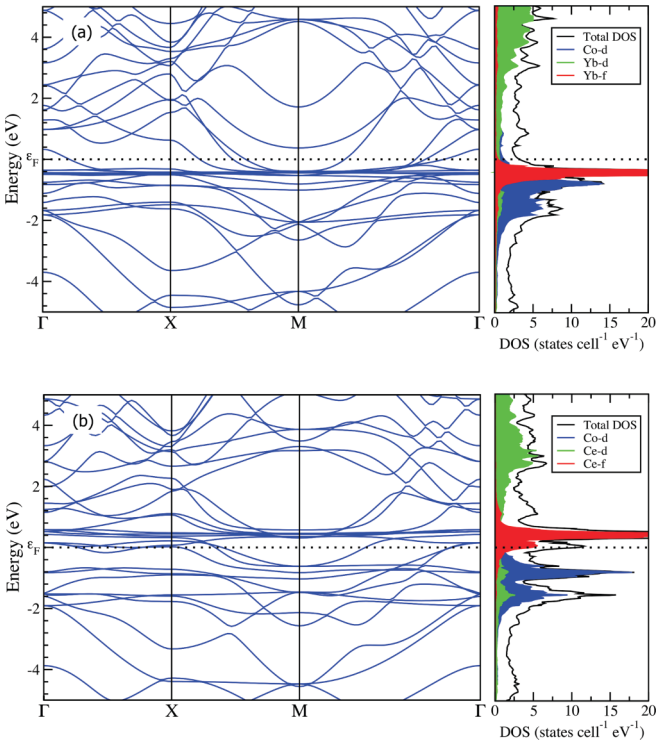


FIG. 8. (Color online) Band structure and density of states (DOS) for (a) $YbCoIn_5$ and (b) $CeCoIn_5$. Only the decomposed DOS for Yb(Ce)-$f$, Yb(Ce)-$d$, and Co-$d$ are shown. Only the total DOS is correctly normalized.

specific heat is observed. This indicates that heavy itinerant quasiparticles still evolve up to such high Yb concentrations and that they even form the superconducting condensate. The latter is evidenced by the observed large anomalies in the specific heat at $T_c$.[4,25] In our dHvA data, however, we cannot resolve any heavy quasiparticle for $x \geqslant 0.2$. A possible reason for that might be a disorder-induced strong scattering making the observation of quantum oscillations in some presumably still existing heavy-electron 4$f$ bands impossible. A likely candidate might be the band that gives rise to the complicated multiconnected Fermi surface resulting in the $\beta$ orbits in $CeCoIn_5$.[34] For both of these orbits, $\beta_1$ and $\beta_2$, we find effective masses of about $53m_e$ at 13 T and $\Theta_{010} = 7^\circ$. For $x = 0.1$, we estimate an effective mass of about $26m_e$ for the $\beta_2$ orbit [Fig. 3(a)] at 32 T. This mass is about a factor of 2 smaller than for pure $CeCoIn_5$, but here a possible field dependence might lead to this mass reduction.[45] From the magnetic-field dependence of the dHvA signals, we can estimate the Dingle temperatures, which are directly proportional to the scattering rates, for the different samples. This, however, can be done reliably only for the orbits giving the strongest dHvA amplitudes. From that, we find that the Dingle temperatures increase from 0.3 K for $CeCoIn_5$ over 0.7 K for $x = 0.1$ to values of about 5.5 K for $x = 0.2$ and 3.5 K for $x = 0.55$. Assuming that the scattering rates are similar for all orbits within one sample, the latter high Dingle temperatures indeed would not allow for a detection of heavy-mass orbits (such as the $\beta$ orbits in $CeCoIn_5$) for $x = 0.2$ and $x = 0.55$.

Anyway, the persistence of the Kondo coherence with even high Yb dilution and the emergence of superconductivity

out of presumed heavy-mass bands with strong disorder is highly unusual. Some ideas on possible cluster formations of strongly correlated Yb impurities have been suggested in order to explain the robust Kondo state and the different evolution of the physical properties of Yb doping versus La doping in $CeCoIn_5$.[26,46] These seem to suggest that the Kondo holes around Yb dopants do not lead to strong additional scattering, which, for example, is the case for La doping.[47] Such an ansatz would allow us to reconcile with the low effective masses and well-resolved dHvA signals in the Yb-rich materials proving their well-ordered crystalline structure.

## IV. CONCLUSION

We performed a comprehensive investigation of the Fermi-surface evolution with Yb substitution in $Ce_{1-x}Yb_xCoIn_5$ via the analysis of dHvA oscillations and the comparison to band-structure calculations. This is a dHvA investigation studying a continuous transition from the heavy-fermion limit ($CeCoIn_5$) to the mixed-valence limit in $YbCoIn_5$ where we prove an Yb valence of $+2.3$. This is further a dHvA study where data could be collected for nearly the entire concentration range in a system with a full lattice of magnetic moments, albeit with two different kinds in this case. The topology change we observe is consistent with what is expected from the band structure. For a small Yb concentration, $x = 0.1$, the band-structure topology and the effective masses remain nearly unchanged compared to $CeCoIn_5$. This contrasts clearly modified Fermi surfaces and light, almost unrenormalized effective masses for $x = 0.2$ and above. These observations cannot explain the heavy-fermion physics observed in specific-heat and resistivity data even for high Yb concentrations. Thus, we postulate the existence of heavy quasiparticles with short mean free paths, not detectable by dHvA experiments. However, the mechanism by which superconductivity can emerge from these charge carriers remains elusive.

## ACKNOWLEDGMENTS

We thank Ingo Opahle and Klaus Koepernik for useful discussions. Part of this work was supported by EuroMagNET II (EU Contract No. 228043) and by the Deutsche Forschungsgemeinschaft. The work in Montreal was financed by the Natural Sciences and Engineering Research Council of Canada (Canada), Fonds Québécois de la Recherche sur la Nature et les Technologies (Québec), and the Canada Research Chair Foundation. Computational resources were provided by Calcul Québec and Compute Canada.

[1] Q. Si and F. Steglich, Science **329**, 1161 (2010).
[2] H. V. Löhneysen, A. Rosch, M. Vojta, and P. Wölfle, Rev. Mod. Phys. **79**, 1015 (2007).
[3] C. Petrovic, P. G. Pagliuso, M. F. Hundley, R. Movshovich, J. L. Sarrao, J. D. Thompson, Z. Fisk, and P. Monthoux, J. Phys.: Condens. Matter. **13**, L337 (2001).
[4] C. Capan, G. Seyfarth, D. Hurt, B. Prevost, S. Roorda, A. D. Bianchi, and Z. Fisk, Europhys. Lett. **92**, 47004 (2010).
[5] V. A. Sidorov, M. Nicklas, P. G. Pagliuso, J. L. Sarrao, Y. Bang, A. V. Balatsky, and J. D. Thompson, Phys. Rev. Lett. **89**, 157004 (2002).
[6] A. Bianchi, R. Movshovich, I. Vekhter, P. G. Pagliuso, and J. L. Sarrao, Phys. Rev. Lett. **91**, 257001 (2003).
[7] J. Paglione, M. A. Tanatar, D. G. Hawthorn, E. Boaknin, R. W. Hill, F. Ronning, M. Sutherland, L. Taillefer, C. Petrovic, and P. C. Canfield, Phys. Rev. Lett. **91**, 246405 (2003).
[8] S. Zaum, K. Grube, R. Schäfer, E. D. Bauer, J. D. Thompson, and H. V. Löhneysen, Phys. Rev. Lett. **106**, 087003 (2011).
[9] L. Howald, G. Seyfarth, G. Knebel, G. Lapertot, D. Aoki, and J.-P. Brison, J. Phys. Soc. Jpn. **80**, 024710 (2011).
[10] See, e.g., S. Paschen, T. Lühmann, S. Wirth, P. Gegenwart, O. Trovarelli, C. Geibel, F. Steglich, P. Coleman, and Q. Si, Nature (London) **432**, 881 (2004).
[11] A. Bianchi, R. Movshovich, N. Oeschler, P. Gegenwart, F. Steglich, J. D. Thompson, P. G. Pagliuso, and J. L. Sarrao, Phys. Rev. Lett. **89**, 137002 (2002).
[12] H. A. Radovan, N. A. Fortune, T. P. Murphy, S. T. Hannahs, E. C. Palm, S. W. Tozer, and D. Hall, Nature (London) **425**, 51 (2003).
[13] A. Bianchi, R. Movshovich, C. Capan, P. G. Pagliuso, and J. L. Sarrao, Phys. Rev. Lett. **91**, 187004 (2003).
[14] P. Fulde and R. A. Ferrell, Phys. Rev. A **135**, 550 (1964).
[15] A. I. Larkin and Y. N. Ovchinnikov, Zh. Eksp. Teor. Fiz. **47**, 1136 (1964) [Sov. Phys. JETP **20**, 762 (1965)].
[16] M. Kenzelmann, T. Strässle, C. Niedermayer, M. Sigrist, B. Padmanabhan, M. Zolliker, A. D. Bianchi, R. Movshovich, E. D. Bauer, J. L. Sarrao, and J. D. Thompson, Science **321**, 1652 (2008).
[17] E. Blackburn, P. Das, M. R. Eskildsen, E. M. Forgan, M. Laver, C. Niedermayer, C. Petrovic, and J. S. White, Phys. Rev. Lett. **105**, 187001 (2010).
[18] G. Zwicknagl and J. Wosnitza, in *BCS: 50 Years*, edited by L. N. Cooper and D. Feldman (World Scientific, Singapore, 2011), pp. 337–371; Int. J. Mod. Phys. B **24**, 3915 (2010).
[19] Y. Kato, C. D. Batista, and I. Vekhter, Phys. Rev. Lett. **107**, 096401 (2011).
[20] J. Paglione, T. A. Sayles, P.-C. Ho, J. R. Jeffries, and M. B. Maple, Nat. Phys. **3**, 703 (2007).
[21] S. K. Goh, J. Paglione, M. Sutherland, E. C. T. O'Farrell, C. Bergemann, T. A. Sayles, and M. B. Maple, Phys. Rev. Lett. **101**, 056402 (2008).
[22] C. Capan, Y.-J. Jo, L. Balicas, R. G. Goodrich, J. F. DiTusa, I. Vekhter, T. P. Murphy, A. D. Bianchi, L. D. Pham, J. Y. Cho, J. Y. Chan, D. P. Young, and Z. Fisk, Phys. Rev. B **82**, 035112 (2010).
[23] Y. Tokiwa, R. Movshovich, F. Ronning, E. D. Bauer, A. D. Bianchi, Z. Fisk, and J. D. Thompson, Phys. Rev. B **82**, 220502(R) (2010).
[24] C. H. Booth, T. Durakiewicz, C. Capan, D. Hurt, A. D. Bianchi, J. J. Joyce, and Z. Fisk, Phys. Rev. B **83**, 235117 (2011).
[25] L. Shu, R. E. Baumbach, M. Janoschek, E. Gonzales, K. Huang, T. A. Sayles, J. Paglione, J. O'Brien, J. J. Hamlin, D. A. Zocco, P.-C. Ho, C. A. McElroy, and M. B. Maple, Phys. Rev. Lett. **106**, 156403 (2011).

[26]E. D. Bauer, Y.-F. Yang, C. Capan, R. R. Urbano, C. F. Miclea, H. Sakai, F. Ronning, M. J. Graf, A. V. Balatsky, R. Movshovich, A. D. Bianchi, A. P. Reyes, P. L. Kuhns, J. D. Thompson, and Z. Fisk, Proc. Natl. Acad. Sci. (USA) **108**, 6857 (2011).

[27]Y.-F. Yang, Z. Fisk, H.-O. Lee, J. D. Thompson, and D. Pines, Nature (London) **454**, 611 (2008).

[28]J. P. Perdew, K. Burke, and M. Ernzerhof, Phys. Rev. Lett. **77**, 3865 (1996).

[29]X. Gonze, B. Amadon, P.-M. Anglade, J.-M. Beuken, F. Bottin, P. Boulanger, F. Bruneval, D. Caliste, R. Caracas, M. Côté *et al.*, Comput. Phys. Commun. **180**, 2582 (2009).

[30]V. I. Zaremba, U. Ch. Rodewald, R.-D. Hoffmann, Y. M. Kalychak, and R. Pöttgen, Z. Anorg. Allg. Chem. **629**, 1157 (2003).

[31]N. Marzari and D. Vanderbilt, Phys. Rev. B **56**, 12847 (1997).

[32]http://www.fplo.de/.

[33]K. Koepernik and H. Eschrig, Phys. Rev. B **59**, 1743 (1999).

[34]R. Settai, H. Shishido, S. Ikeda, Y. Murakawa, M. Nakashima, D. Aoki, Y. Haga, H. Harima, and Y. Onuki, J. Phys.: Condens. Matter **13**, L627 (2001).

[35]A. McCollam, S. R. Julian, P. M. C. Rourke, D. Aoki, and J. Flouquet, Phys. Rev. Lett. **94**, 186401 (2005).

[36]The data for $\Theta_{001}$ rotations are only shown for $x = 1$ and 0.55. For other concentrations very similar, almost angular-independent dHvA frequencies are observed. For rotations from $c$ to [110] the angular dependences of the dHvA signals are very similar to the $\Theta_{010}$ rotations (data not shown).

[37]S. Elgazzar, I. Opahle, M. Richter, and P. M. Oppeneer, Phys. Rev. B **77**, 125105 (2008).

[38]I. M. Lifshitz and A. M. Kosevich, Zh. Eksp. Teor. Fiz. **29**, 730 (1955) [Sov. Phys. JETP **2**, 636 (1956)].

[39]D. Shoenberg, *Magnetic Oscillations in Metals* (Cambridge University Press, Cambridge, UK, 1984).

[40]For the data shown in Fig. 7 for $x = 0.1$ at $\Theta_{010} = 14^\circ$, the effective mass corresponds to a dHvA frequency of 4.5 kT that is a mixture of the $\alpha_2$ and $\alpha_3$ orbits. From the Grenoble data, we obtain an effective mass for the $\alpha_2$ orbit of $8.6m_e$ at $\Theta_{010} = 3^\circ$ and 32 T.

[41]Only for two orbits effective masses larger than $2m_e$ are found, i.e., $2.4m_e$ for $F_6$ in $x = 0.85$ and $2.6m_e$ for $F_{13}$ in $x = 0.55$.

[42]The limited temperature range below 1 K did not allow to determine the effective masses with high accuracy. However, the very small amplitude reduction of the dHvA signal proves that all orbits in the sample with $x = 0.2$ have light effective masses.

[43]B. Amadon, F. Jollet, and M. Torrent, Phys. Rev. B **77**, 155104 (2008).

[44]B. Amadon, F. Lechermann, A. Georges, F. Jollet, T. O. Wehling, and A. I. Lichtenstein, Phys. Rev. B **77**, 205112 (2008).

[45]Indeed, for the limited magnetic-field range over which we observed the $\beta_2$ orbit we found indications for a mass reduction with increasing field between 30 and 35 T.

[46]M. Dzero and X. Huang, J. Phys.: Condens. Matter **24**, 075603 (2012).

[47]N. Harrison, U. Alver, R. G. Goodrich, I. Vekhter, J. L. Sarrao, P. G. Pagliuso, N. O. Moreno, L. Balicas, Z. Fisk, D. Hall, R. T. Macaluso, and J. Y. Chan, Phys. Rev. Lett. **93**, 186405 (2004).